Supporting Information

Selective C$_{2+}$ Alcohol Synthesis from CO$_2$ Hydrogenation via Reaction-Coupling Strategy

Yanqiu Wang[1], Di Xu[2], Xinxin Zhang[1], Xinlin Hong[1]* and Guoliang Liu[1]*

[1]College of Chemistry and Molecular Sciences, Wuhan University, Wuhan 430072, P. R. China.

[2]School of Power and Mechanical Engineering, Wuhan University, Wuhan 430072, P. R. China

* Corresponding authors. Email address: liugl@whu.edu.cn; hongxl@whu.edu.cn
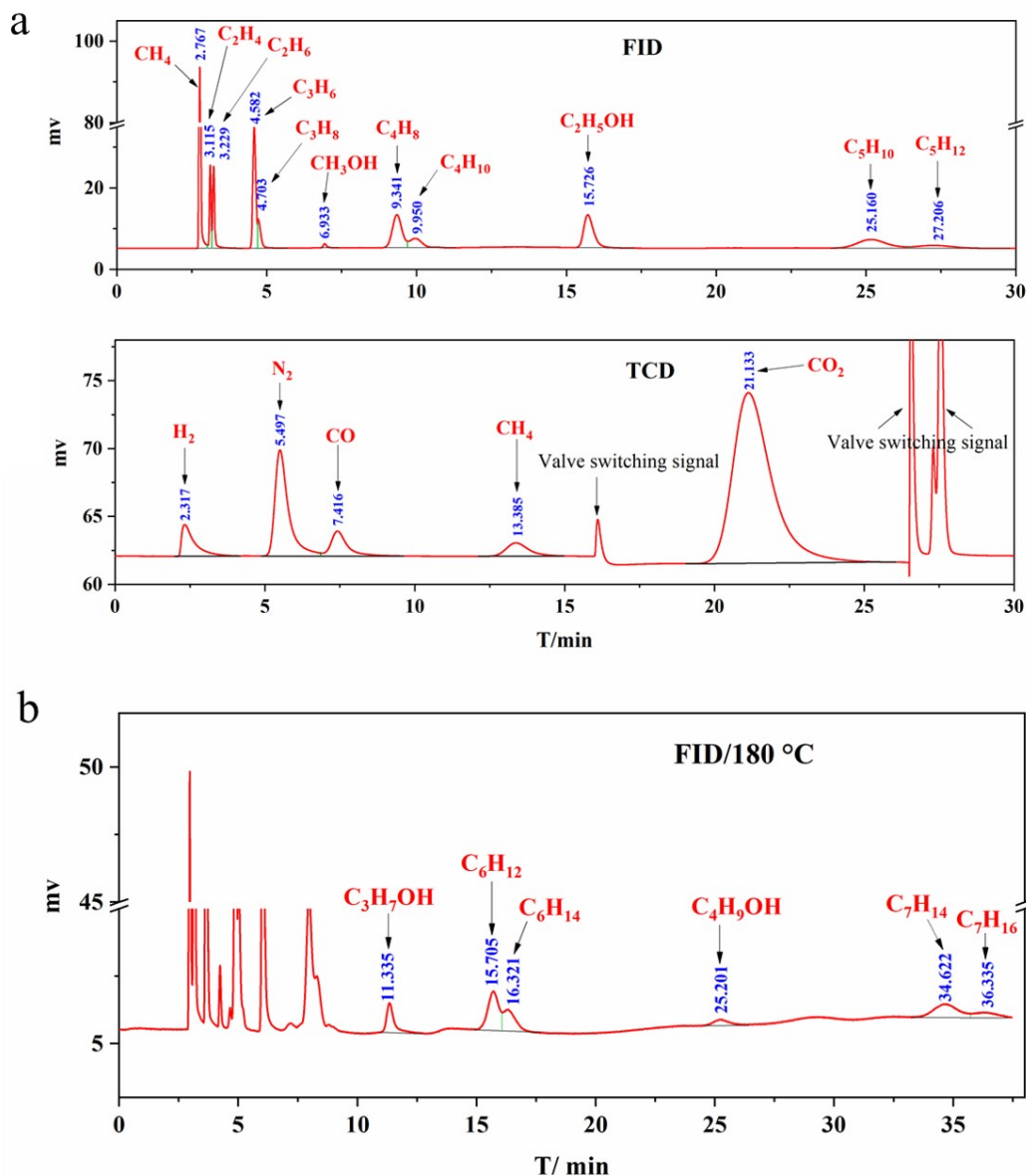
Fig S1. (a) FID and TCD signal at chromatographic column temperature of 130 °C and (b) FID signal at chromatographic column temperature of 180 °C.

In order to distinguish alkanes and alkenes, the chromatographic column temperature was initially set at 130 °C. When the reaction was in equilibrium, the TCD detector can record H_2, N_2, CO, CH_4, and CO_2 and the FID detector can record methanol, ethanol and C_1-C_5 hydrocarbons. Then, the chromatographic column temperature was set at 180 °C to record higher boiling point products including C_3H_7OH, C_4H_9OH and C_6-C_7 hydrocarbons

The CO_2 conversion, products selectivity and carbon balance were calculated according to the equations 1~4 as follows:

(1) CO_2 conversion was calculated according to:

$$CO_2 \text{ conversion} = \frac{CO_{2\ in} - CO_{2\ out}}{CO_{2\ in}} \times 100\% \qquad (Eq\ 1)$$

Where $CO_{2\ in}$ and $CO_{2\ out}$ denote the moles of CO_2 at the inlet and outlet, respectively.

(2) CO selectivity was calculated according to the following equation:

$$\text{CO selectivity} = \frac{\dfrac{CO_{out}}{CO_{2\,in} - CO_{2\,out}} \times 100\%}{\quad} \qquad \text{(Eq 2)}$$

Where CO_{out} denotes the mole of CO at the outlet.

(3) Hydrocarbons or higher alcohols (i) selectivity was calculated according to the following equation:

$$\text{Selectivity} = \frac{N_i \times n_{i,\,out}}{\sum (N_i \times n_{i,\,out})} \times 100\% \qquad \text{(Eq 3)}$$

Where N_i and n_i represent the mole and carbon number of product i.

(4) The carbon banlance was calculated according to the following:

$$\text{Carbon balance} = \frac{CO_{2\,out} + CO_{out} + \sum (N_i \times n_{i,\,out})}{CO_{2\,in}} \times 100\% \qquad \text{(Eq 4)}$$
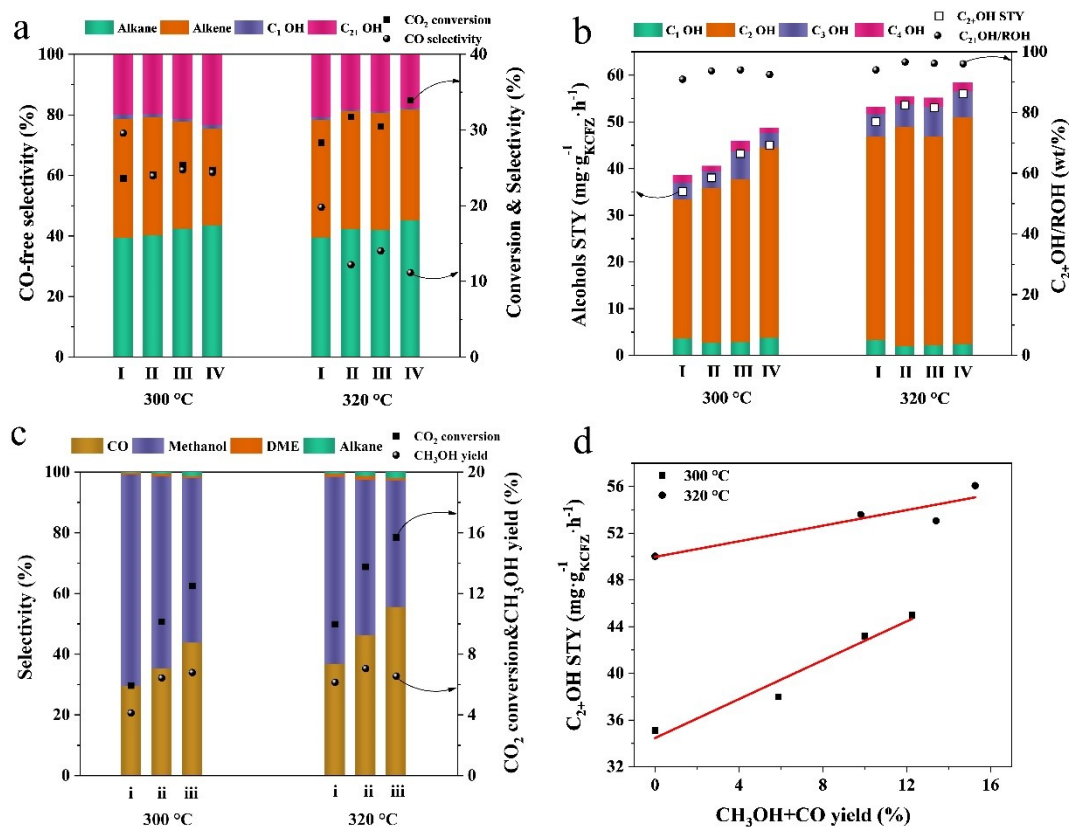
Fig. S2. (a, b) Catalytic performance of CO_2 hydrogenation over sole 6.4KCFZ (I) and 6.4KCFZ/xCuZnZr (II: 6.4KCFZ/ZnZr, III: 6.4KCFZ/0.5CuZnZr, and IV: 6.4KCFZ/0.7CuZnZr) with mass ratio of 2/1 and powder mixing method. (a) CO_2 conversion, CO selectivity, and CO-free selectivity to organic products (mol %) and (b) distribution of alcohols in STY based on the mass of 6.4KCFZ catalyst and weight fraction of $C_{2+}OH$ in total alcohols; (c) CO_2 hydrogenation performance of xCuZnZr catalysts (i: ZnZr, ii: 0.5CuZnZr, and iii: 0.7CuZnZr) including CH_3OH and CO selectivity, CO_2 conversion and CH_3OH yield; (d) Correlation between $C_{2+}OH$ STY of multifunctional catalysts and CH_3OH plus CO yield over the corresponding xCuZnZr catalysts at 300 °C and 320 °C. Reaction conditions: catalyst mass = 0.3 g except for 0.2 g for sole 6.4KCFZ catalyst, 5 MPa, $H_2/CO_2/N_2$ = 72/24/4, and 15 mL min^{-1}.

In order to further study the influence of CH_3OH/CO produced by additional catalysts in HAS. A series of xCuZnZr catalysts were then integrated with 6.4KCFZ by powdering mixing method. ZnZr solid solution is a highly selective and stable methanol synthesis catalyst [1]. Introducing a small amount of Cu (0.5%, 0.7%) into ZnZr forming a ternary metal oxide solid solution can promote CH_3OH production in CO_2 hydrogenation. The promoted activity attributed to the enhancement of hydrogenation capacity from Cu and accelerated transformation of HCOO* to CH_3O* caused by the hydrogen spillover effect [2]. When adding xCuZnZr catalysts in 6.4KCFZ, the multifunctional catalyst all show improved CO_2 conversion and HA STY and decreased CO selectivity (a, b). And $C_{2+}OH$ fraction in alcohols doesn't change much. It seems that compared to 320 °C, the change of HA STY is more sensitive to the amount of CH_3OH and CO produced from xCuZnZr at 300 °C. This result indicates the xCuZnZr catalysts affording CH_xO*/CO species can promote HA production kinetically.
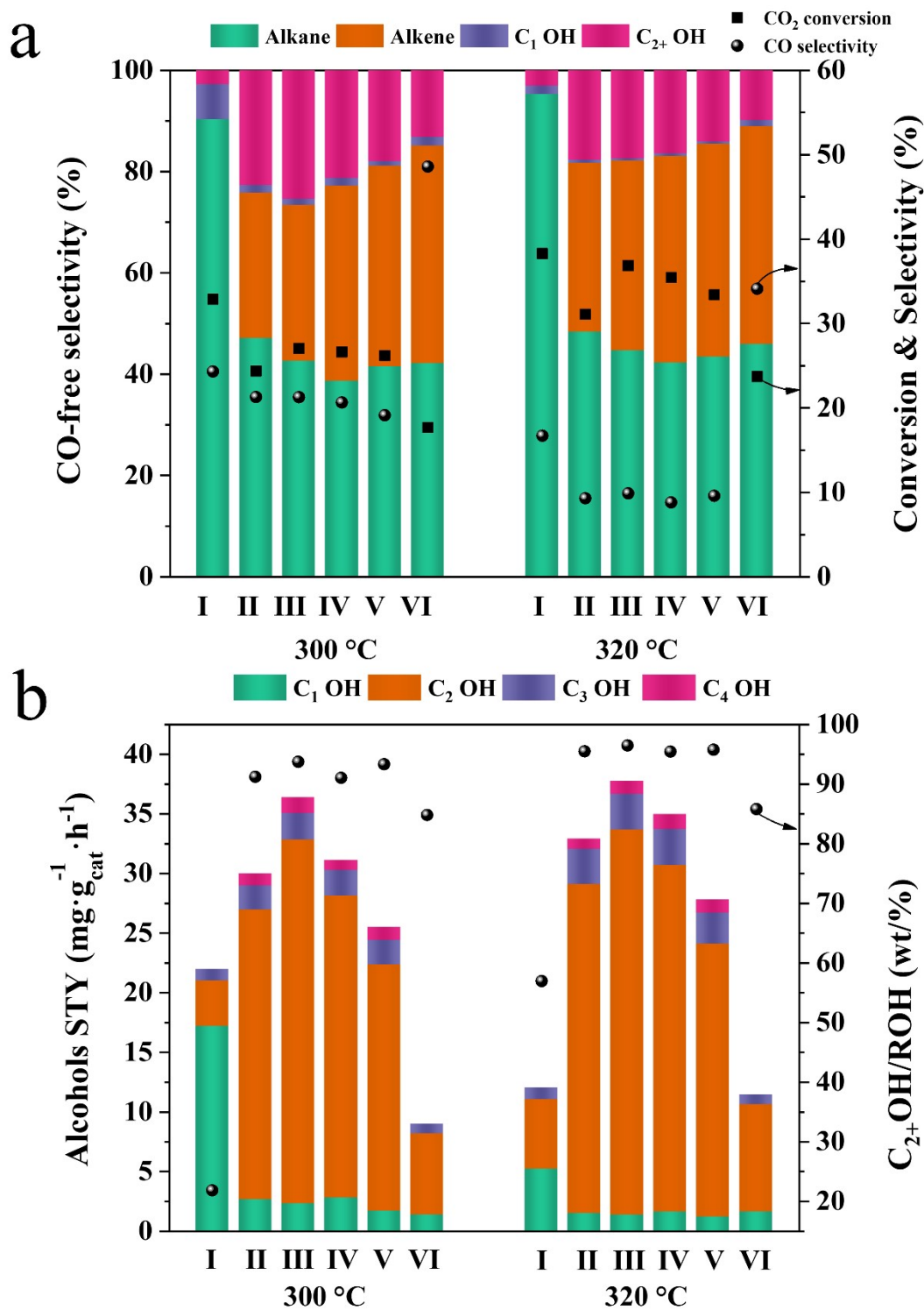
Fig. S3. Catalytic performance of CO₂ hydrogenation over *x*KCFZ catalysts (I: 0.1KCFZ, II: 3.0KCFZ, III: 4.7KCFZ, IV: 6.4KCFZ, V: 10.7KCFZ, VI: 17.2KCFZ). (a) CO₂ conversion, CO selectivity, and CO-free selectivity to organic products (mol %) and (b) distribution of alcohols in STY and weight fraction of $C_{2+}OH$ in total alcohols. Reaction conditions: catalyst mass = 0.3 g, 5 MPa, $H_2/CO_2/N_2$ = 72/24/4, 300 and 320 °C, and 3 L g_{cat}^{-1} h⁻¹.

Table S1. Comparison of HAS activity from CO_2 hydrogenation over KCFZ/CuZnAlZr multifunctional catalyst with some advanced catalysts.

Catalyst	P (MPa)	T (ºC)	WHSV (L g_{cat}^{-1} h^{-1})	CO_2 Conv.(%)	CO Select.(%)	HA Select.(%)	HA STY (mg g_{cat}^{-1} h^{-1})	Ref.
4.6K-CMZF	5	320	6	30.4	30.6	15.7	69.6	[3]
Cs-CFZ	5	330	4.5	36.6	20.6	19.8	73.4	[4]
CZA/K-CMZF	5	320	3	46.0	9.6	19.5	64.9	[5]
RhFeLi-TiO_2	3	250	6	15.7	12.5	31.3(ethanol)	24.2(ethanol)	[6]
Cu/Co_3O_4-2h	3	250	36	13.9	6.5	15.2(ethanol)	86.0(ethanol)	[7]
Na-Co/SiO_2	5	250	6	21.5	26.3	12.5(ROH)	0.47(mmol g_{cat}^{-1} h^{-1})	[8]
Cu@Na-Beta	2.1	300	12	18.0	21	79.0	398	[9]
CZK(1.5)//CFCK(4.5)	6	350	5	32.4	45.3	11.8 (ROH)	72.4	[10]
NaFe@C/KCuZnAl	5	320	4.5	39.2	9.4	31.7(ethanol)	--	[11]
CuZn$Fe_{0.5}K_{0.15}$	6	300	5	42.3	49.2	36.7 (ROH)	148.1 (mg mL_{cat}^{-1} h^{-1})	[12]
FeNaS-0.6	3	320	8	32.0	20.7	12.8	78.5	[13]
Co/$La_4Ga_2O_9$	3.5	270	3	4.6	15.4	34.7	--	[14]
$Mo_1Co_1K_{0.8}$	12	320	3	28.8	56.3	4.8	--	[15]
$Mo_1Co_1K_{0.6}$-AC-185 %	5	320	3	8.1	69.8	4.8	--	[16]
4.7KCFZ/CuZnAlZr (1:1)	5	300	3	27.0	25.4	24.6	42.0	This work
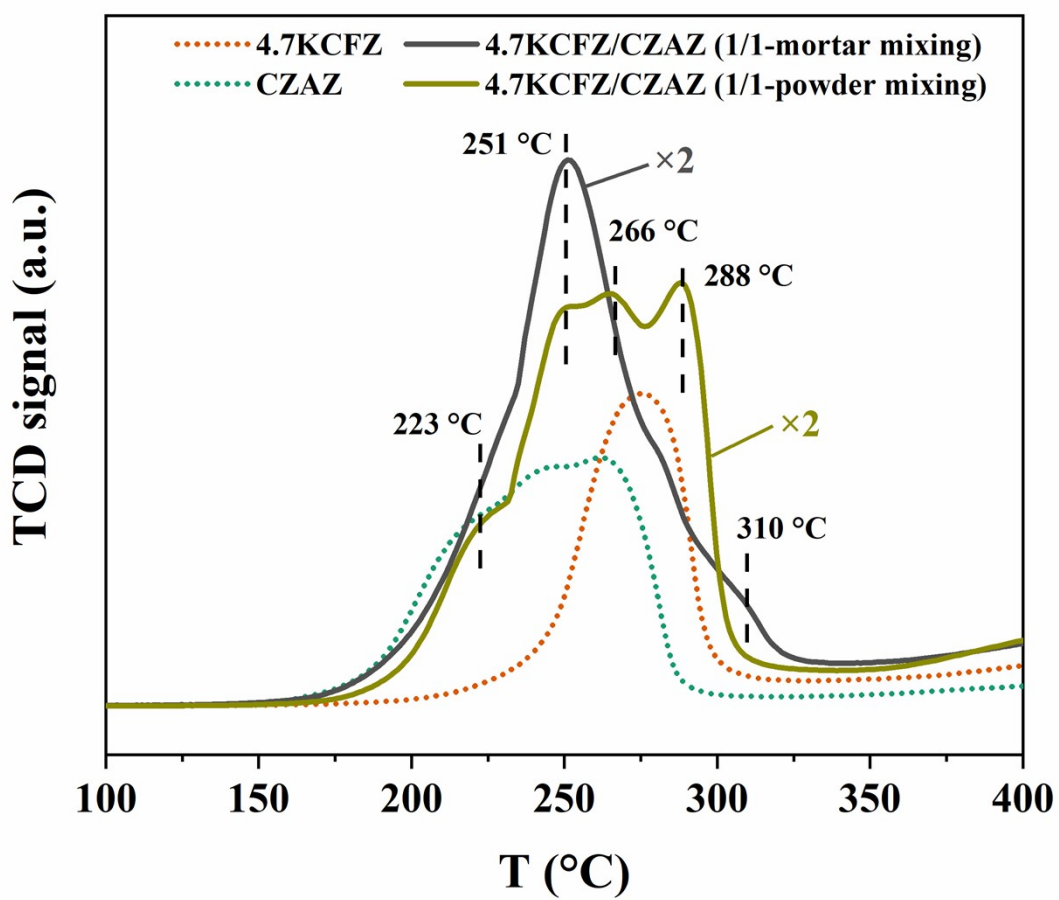
Fig. S4. H_2-TPR results over the sole 4.7KCFZ, CuZnAlZr catalysts, and multifunctional catalysts with mortar mixing and powder mixing.
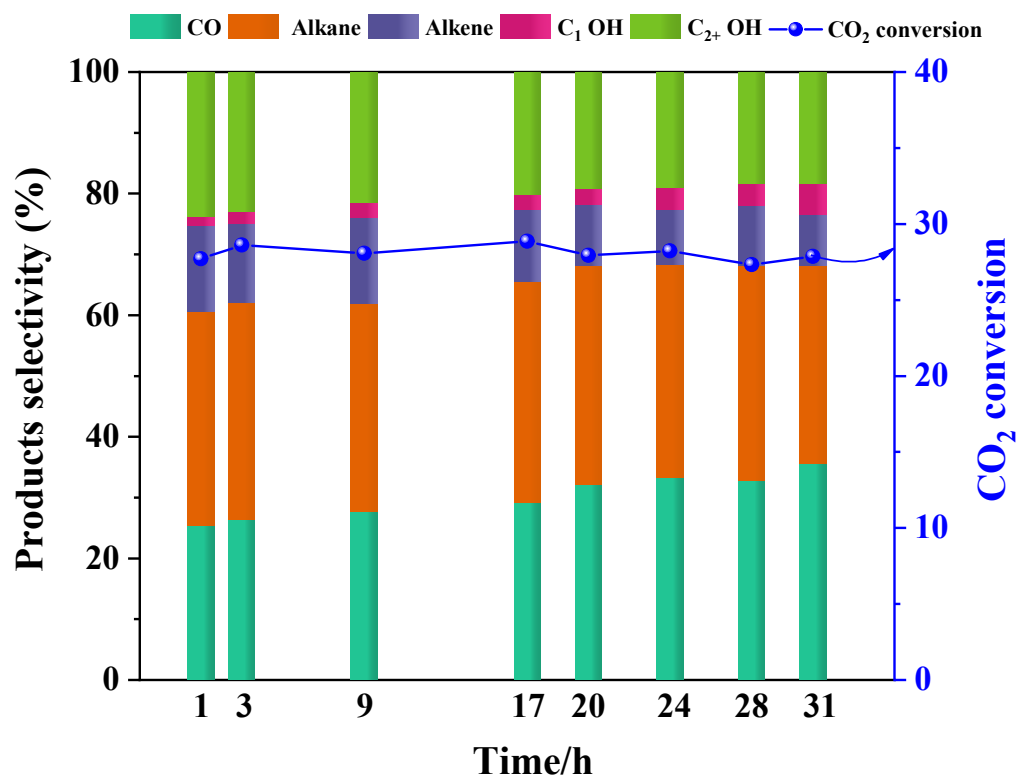
Fig. S5. Time-on-stream test of the 4.7KCFZ/CuZnAlZr (1/1-mortar mixing) multifunctional catalyst. Reaction conditions: catalyst mass = 0.3 g, 5 MPa, $H_2/CO_2/N_2$ = 72/24/4, 3 L g_{cat}^{-1} h^{-1}, 300 °C.

Before the TOS test, the catalyst was reduced in 10% H_2/Ar flow and activated in CO_2/H_2 flow of 15 mL min^{-1} at 5 MPa and 320 °C for 3 h. And then decrease the reaction temperature to 300 °C.

Table S2. Effect of reaction pressure on the catalytic performance of CO_2 hydrogenation over 4.7KCFZ/CuZnAlZr (1/1-mortar mixing) multifunctional catalyst[a].

Reaction pressure	CO_2 Conv. (%)	CO Select. (%)	Products selectivity (mol%)				$C_{2+}OH/ROH$ (wt)	$C_{2+}OH$ STY (mg g_{cat}^{-1} h^{-1})
			RH[b]	RH[=c]	C_1OH	$C_{2+}OH$		
3	24.9	37.5	46.6	27.0	2.5	23.9	86.8	26.2
5	29.4	26.1	42.7	24.0	2.1	31.2	91.3	42.5
7	34.1	14.4	52.9	18.9	2.2	26.0	89.2	53.7

[a]Reaction conditions: $H_2/CO_2/N_2$ = 72/24/4, 300 °C and 3 L g_{cat}^{-1} h^{-1}.

[b]RH: Paraffins. [c]RH=: Olefins.

As shown in Table S1, high pressure is beneficial to the conversion of CO_2 and the production of alcohols and hydrocarbons.
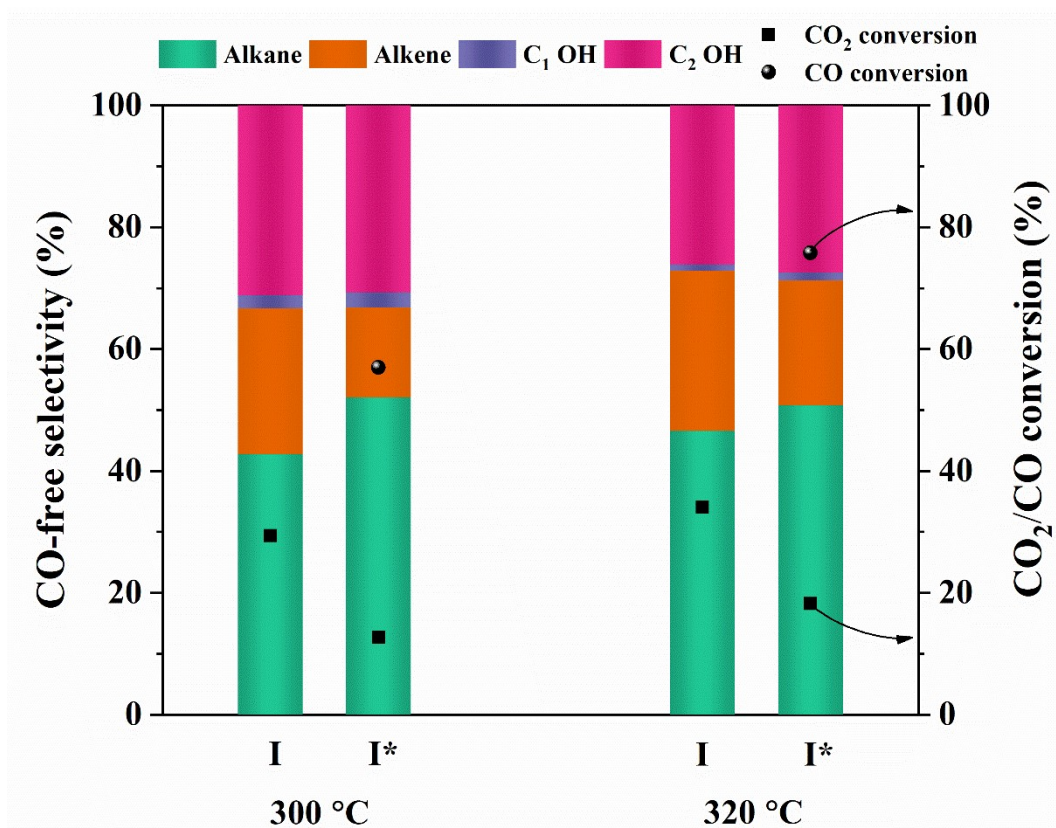
Fig. S6. CO_2/CO conversion and other products selectivity toward alkanes, alkenes, methanol, and C_{2+} alcohols of 4.7KCFZ/ CuZnAlZr (1/1-mortar mixing) multifunctional catalyst under $CO_2/H2$ (I) and $CO_2/CO/H_2$ (I*). Reaction conditions: catalyst mass = 0.3 g, 5 MPa, 300 °C, 3 L g_{cat}^{-1} h^{-1}, $H_2/CO_2/N_2$ = 72/24/4, and $H_2/CO_2/CO/N_2$ = 72/20/4/4 (I*).

The CO_2 conversion and CO conversion were calculated by the following eqs 1−2

$$CO_2 \text{ conversion} = \frac{CO2_{in} - CO2_{out}}{CO2_{in}} \times 100\% \qquad (1)$$

$$CO \text{ conversion} = \frac{CO_{in} - CO_{out}}{CO_{in}} \times 100\% \qquad (2)$$
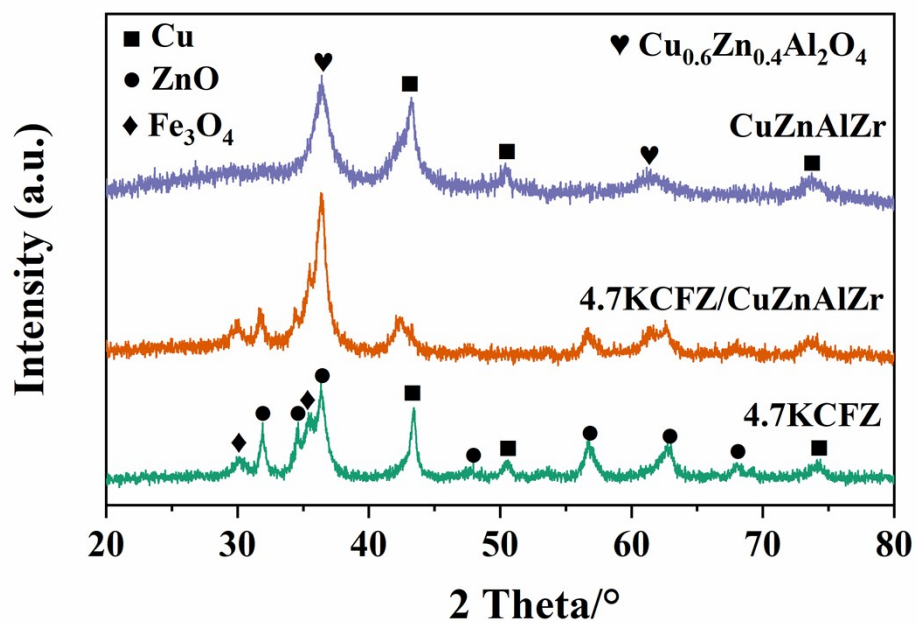
Fig. S7. XRD patterns of reduced 4.7KCFZ, CuZnAlZr, and 4.7KCFZ/CuZnAlZr (1/1-mortar mixing) catalysts.
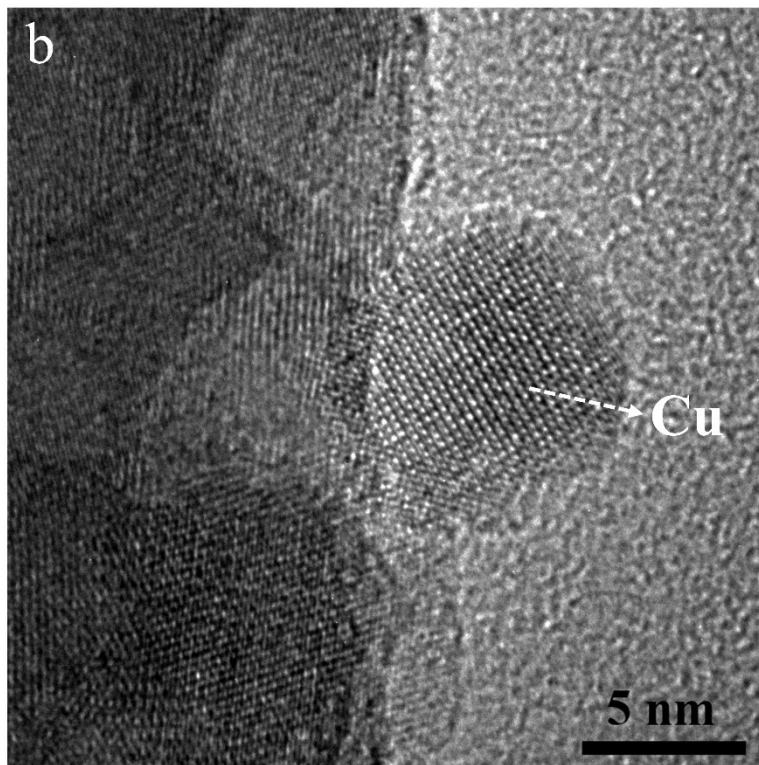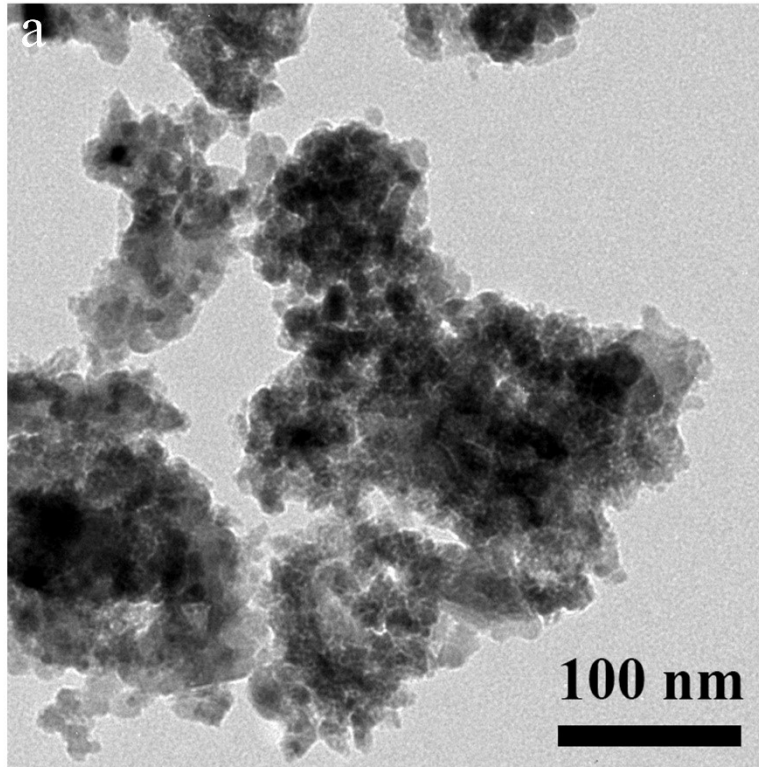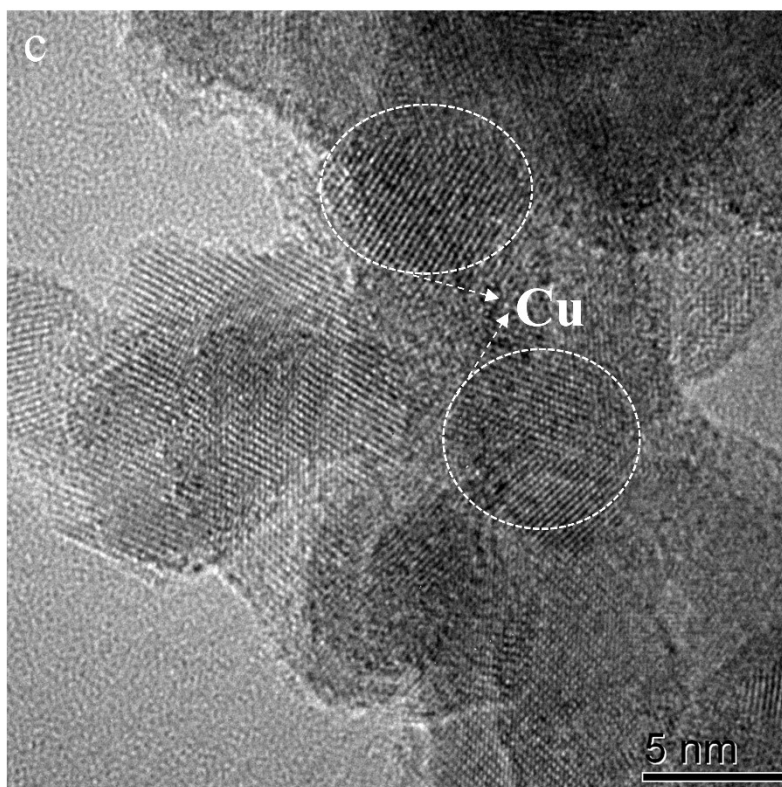
Fig. S8. TEM (a) and HRTEM (b and c) images of reduced 4.7KCFZ/CuZnAlZr (1/1-mortar mixing) catalyst.

a

100 nm

b

Cu (111)
0.208 nm

ZnO (101)
0.249 nm

5 nm
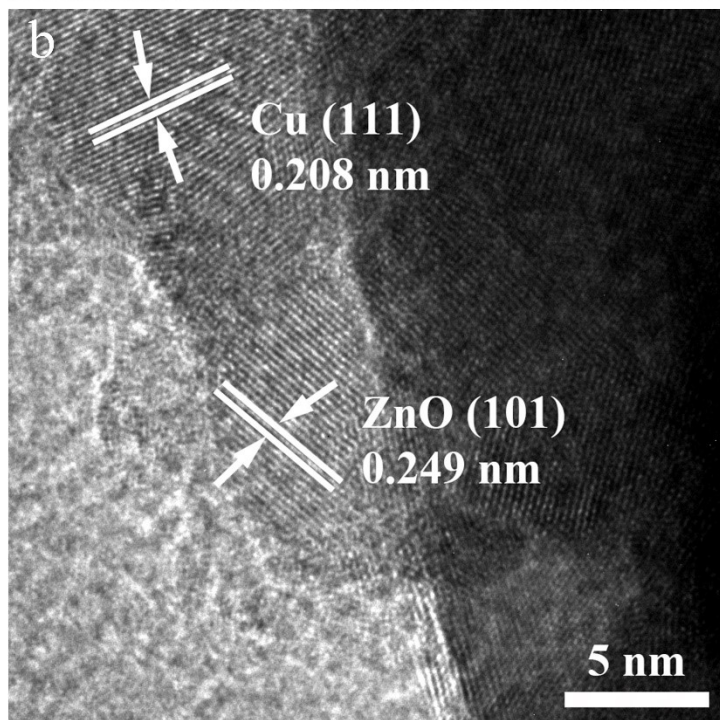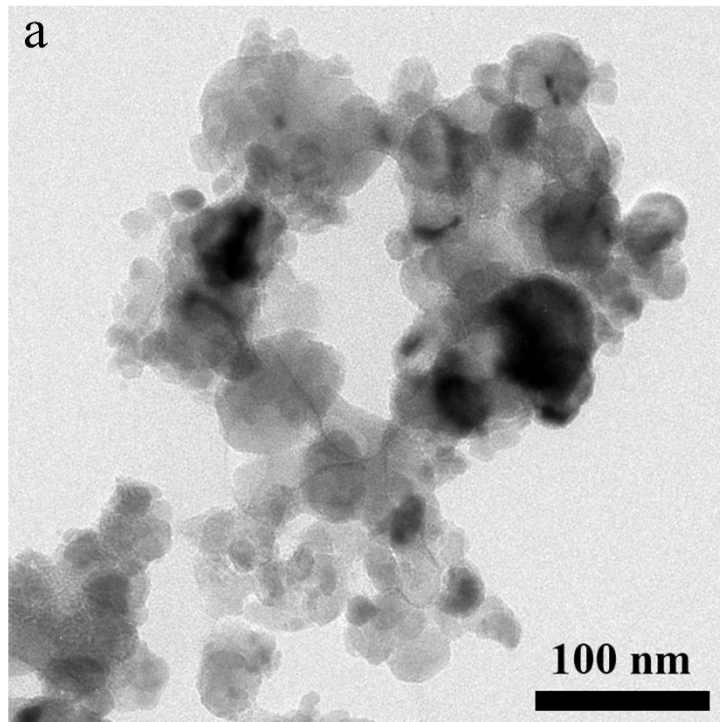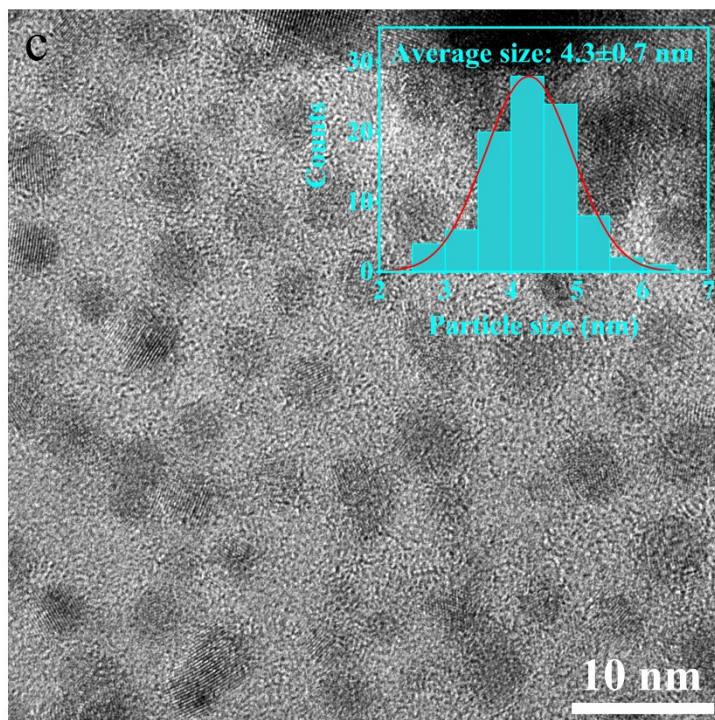
Fig. S9. TEM (a) and HRTEM (b and c) images of spent 4.7KCFZ/CuZnAlZr (1/1-mortar mixing) catalyst and the corresponding histogram of Cu particle size distribution (inset).

The Cu particle size in spent catalysts is about 4.3 nm. Compared with reduced catalyst, Cu particles did not change significantly.

Table S3. Physical properties of the sole and multifunctional catalysts obtained from N_2

	S_{BET}^a ($m^2 g^{-1}$)	V_m^b ($cm^3 g^{-1}$)	d_{pore}^c (nm)
4.7KCFZ	35.2	0.186	18.6
CuZnAlZr	40.9	0.338	29.3
4.7KCFZ/CuZnAlZr (1/1-mortar mixing)	49.1	0.264	19.9

desorption isotherms.
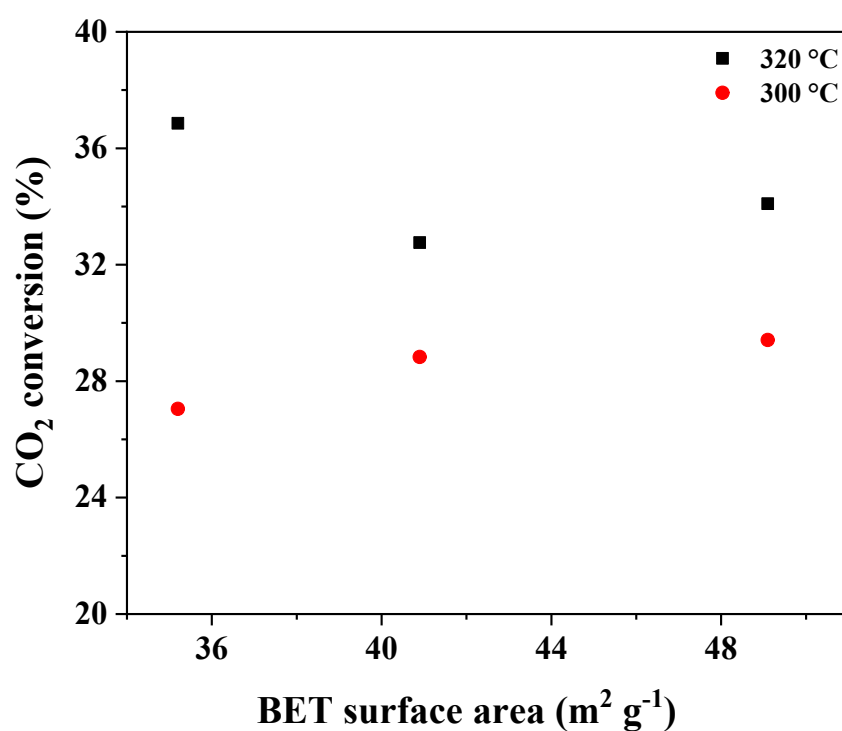
Fig. S10. CO_2 conversion at 300 and 320 ºC as a function of the BET surface area of the sole 4.7KCFZ, CuZnAlZr and 4.7KCFZ/CuZnAlZr (1/1-mortar mixing) multifunctional catalysts.
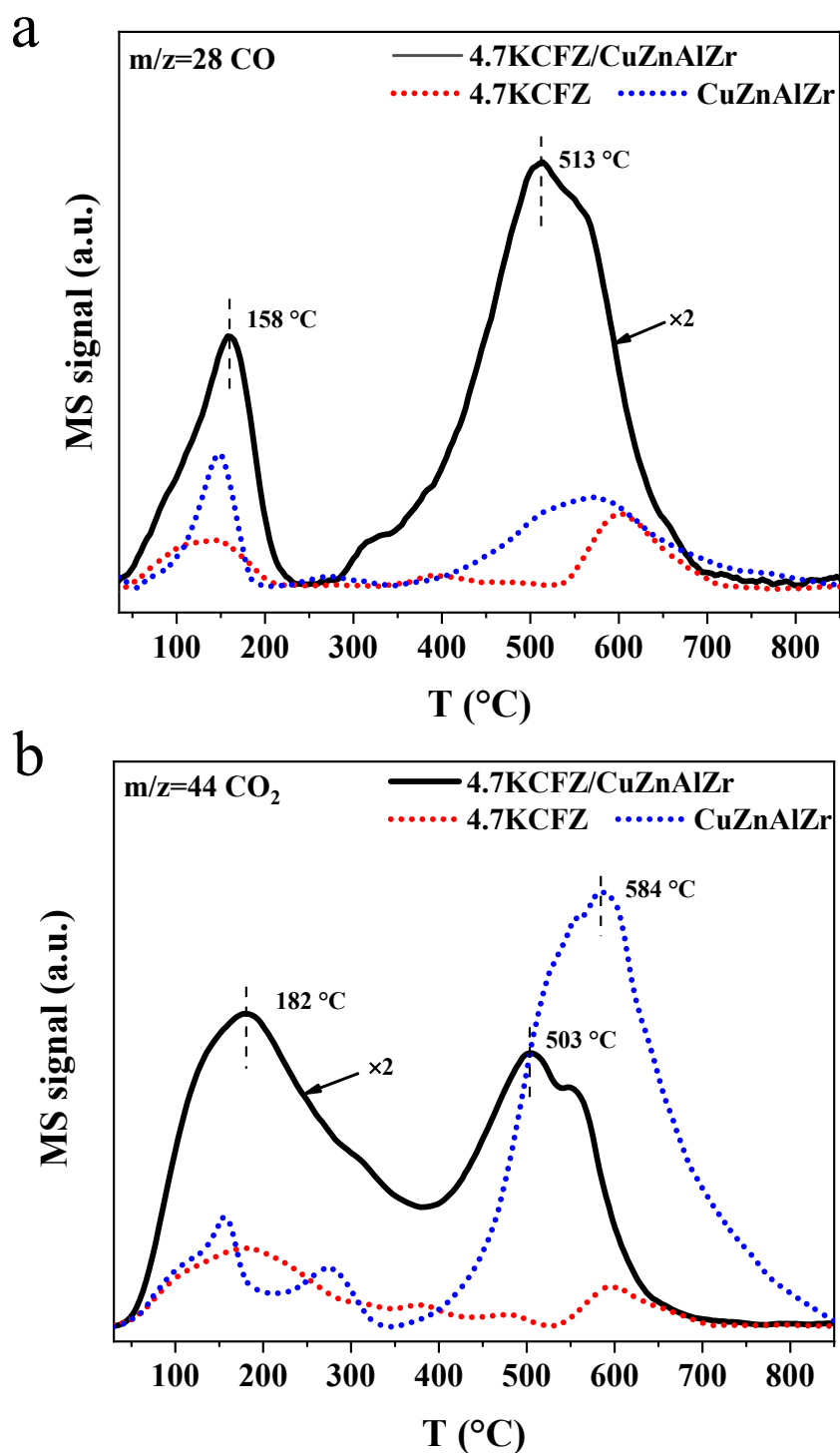
Fig. S11. MS signals of (a) m/z = 28 and (a) m/z = 44 in CO pre-desorbed CuZnAlZr, 4.7KCFZ and 4.7KCFZ/CuZnAlZr (1/1-mortar mixing) catalysts under Ar flow.

CO chemisorption tests were then performed to further investigate the synergetic effect between 4.7KCFZ and CuZnAlZr. Fig. S9a and 9b show the CO-TPD results over the sole catalysts and multifunctional catalysts. The signal of m/z = 28 (CO) represents the adsorption of CO on the

catalyst surface. There are two kinds of adsorption strength of CO in 100-800 °C, one is weak adsorption at about 150 °C and the other is strong adsorption at about 300-700 °C. The adsorption capacity of CO on multifunctional catalysts increases significantly than two sole components. This indicates the catalyst shows stronger CO adsorption strength with a synergy between CuZnAlZr and 4.7KCFZ. The signal of CO_2 (m/z = 44) can be detected due to the reaction between adsorbed CO and surface O species (Fig. S9b). The desorption temperature of CO_2 is the performance of CO activation ability. CuZnAlZr shows strong and high CO_2 desorption at high temperatures (about 584 °C) that is the reason why it has strong WGSR ability. After introducing the CuZnAlZr component, the CO activation ability in 4.7KCFZ/CuZnAlZr multifunctional catalyst is improved observably in the reaction temperature range.
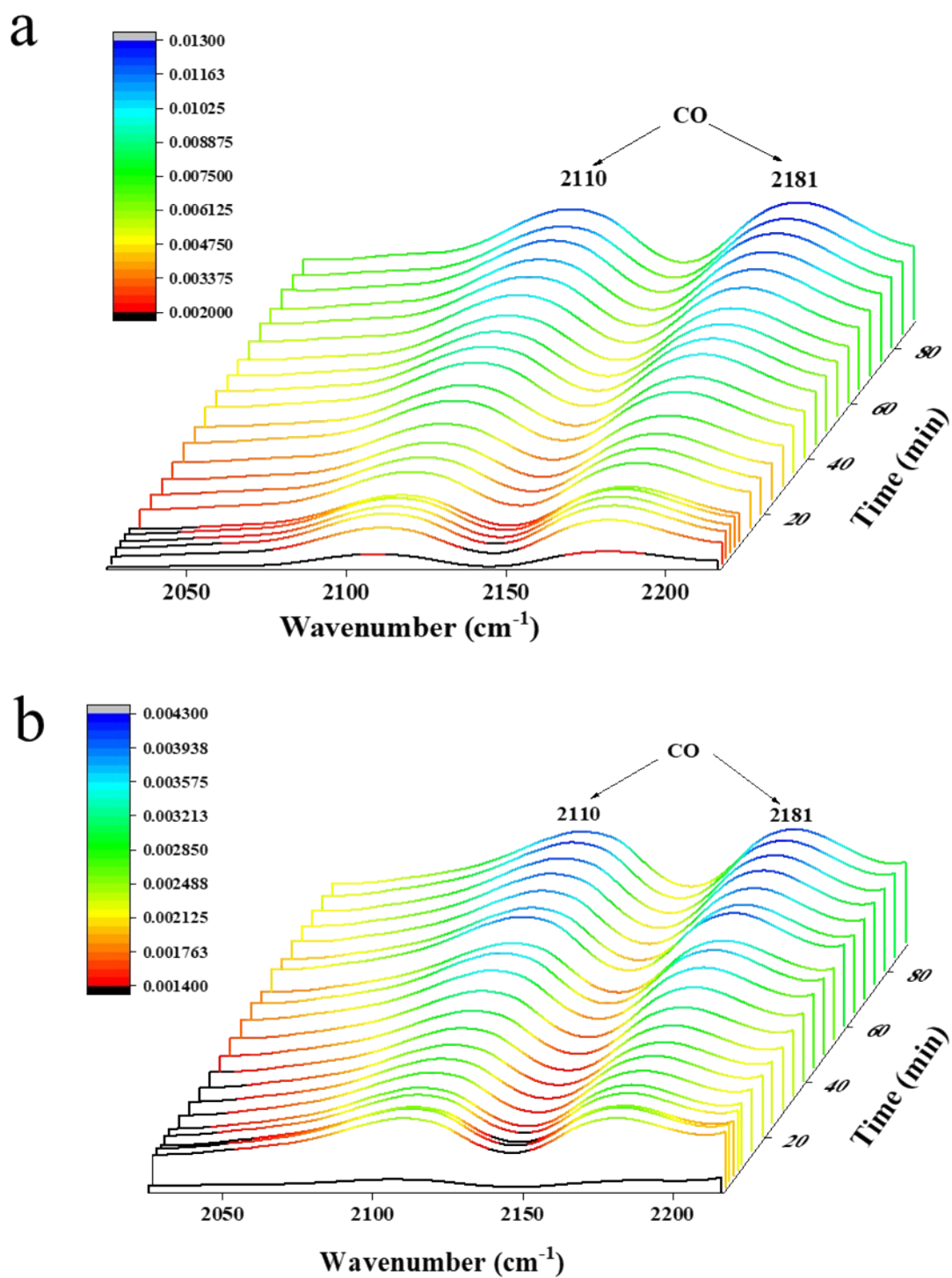
Fig S12. DRIFTS spectra at the range of 2025-2217 cm^{-1} over (a) KCFZ and (b)KCFZ/ZnZr catalysts in $CO_2 + H_2$ flow for 90 min;

Reaction conditions: 0.3 MPa, $CO_2/H_2 = 1/3$, 15 mL/min, 250 °C.
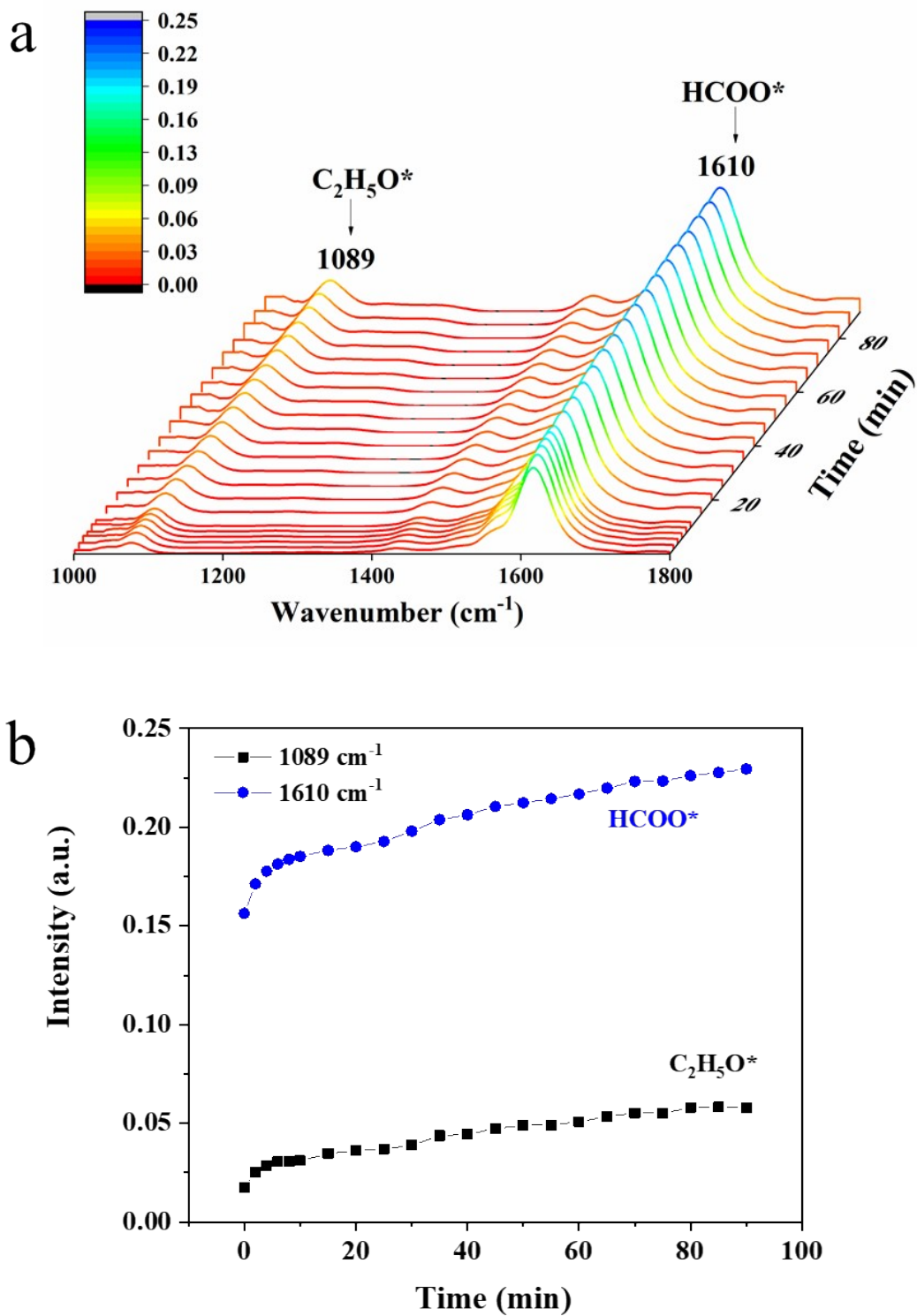
Fig S13. (a) In situ DRIFTS spectra during 1000-1800 cm^{-1} of surface species on KCFZ and (b) dynamic IR peak intensity change of $C_2H_5O^*$ (1089 cm^{-1}), HCOO* 1610 cm^{-1}).
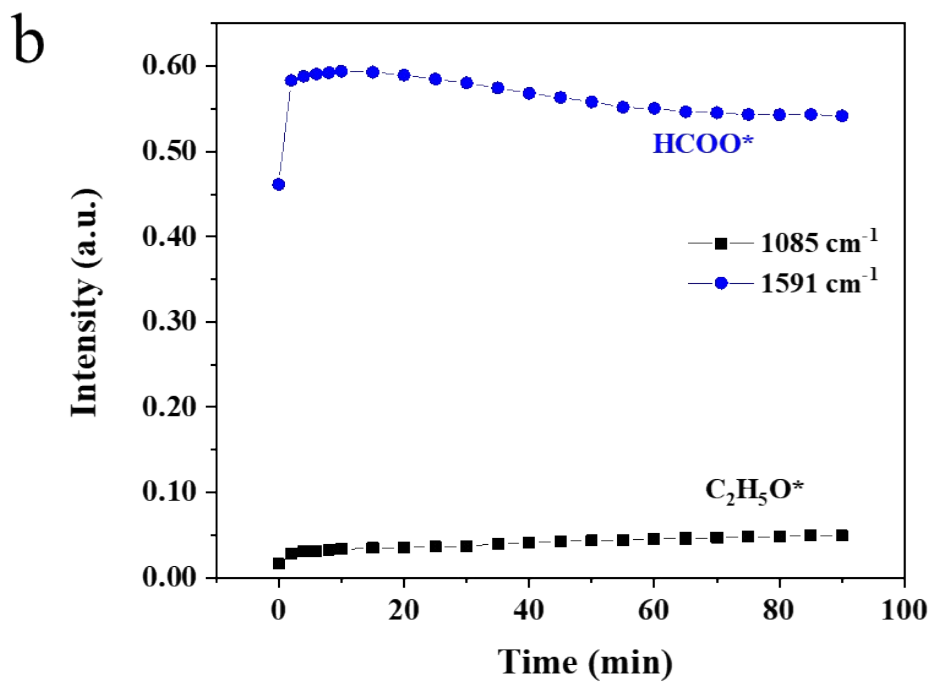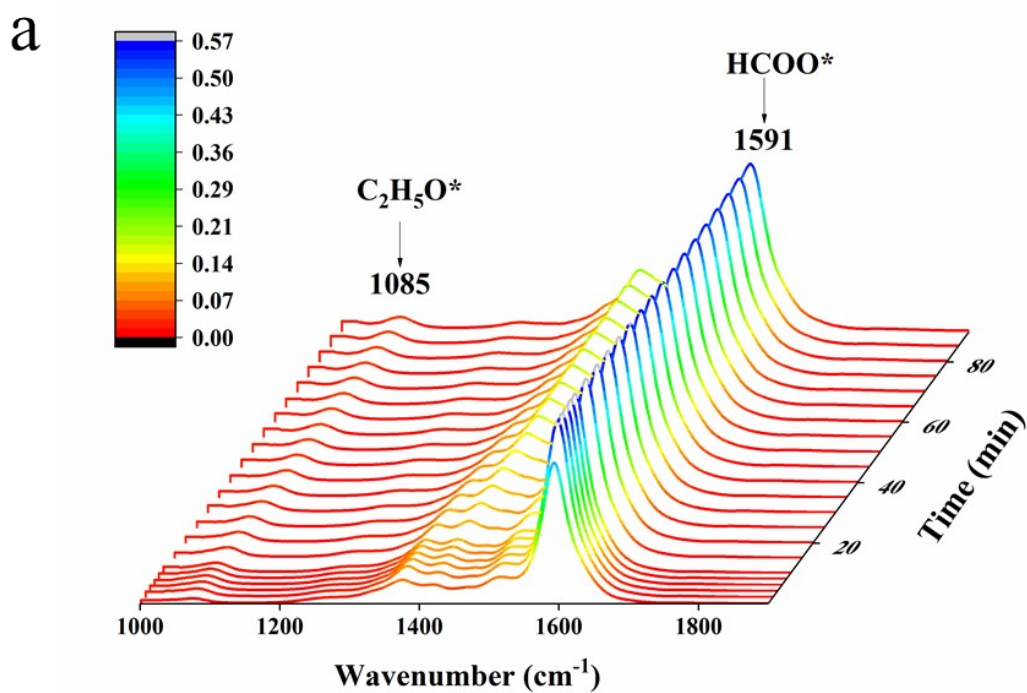
Fig S14. (a) In situ DRIFTS spectra during 1000-1850 cm^{-1} of surface species on KCFZ/ZnZr and (b) dynamic IR peak intensity change of C_2H_5O* (1085 cm^{-1}), HCOO* (1591 cm^{-1}).

References

1.   J. Wang, G. Li, Z. Li, C. Tang, Z. Feng, H. An, H. Liu, T. Liu and C. Li, *Sci. Adv.*, 2017, **3**, e1701290.
2.   D. Xu, X. Hong and G. Liu, *J. Catal.*, 2021, **393**, 207-214.
3.   D. Xu, M. Ding, X. Hong and G. Liu, *ACS Catal.*, 2020, **10**, 14516-14526.
4.   D. Xu, M. Ding, X. Hong, G. Liu and S. C. E. Tsang, *ACS Catal.*, 2020, **10**, 5250-5260.
5.   D. Xu, H. Yang, X. Hong, G. Liu and S. C. E. Tsang, *ACS Catal.*, 2021, **11**, 8978-8984.
6.   M. R. Gogate and R. J. Davis, *Catal. Commun.*, 2010, **11**, 901-906.
7.   C. Yang, S. Liu, Y. Wang, J. Song, G. Wang, S. Wang, Z.-J. Zhao, R. Mu and J. Gong, *Angew. Chem. Int. Ed.*, 2019, **58**, 11242-11247.
8.   S. Zhang, Z. Wu, X. Liu, Z. Shao, L. Xia, L. Zhong, H. Wang and Y. Sun, *Appl. Catal., B*, 2021, **293**, 120207.
9.   L. Ding, T. Shi, J. Gu, Y. Cui, Z. Zhang, C. Yang, T. Chen, M. Lin, P. Wang, N. Xue, L. Peng, X. Guo, Y. Zhu, Z. Chen and W. Ding, *Chem*, 2020, **6**, 2673-2689.
10.   H. Guo, S. G. Li, F. Peng, H. Zhang, L. Xiong, C. Huang, C. Wang and X. Chen, *Catal. Lett.*, 2015, **145**, 620-630.
11.   Y. Wang, K. Wang, B. Zhang, X. Peng, X. Gao, G. Yang, H. Hu, M. Wu and N. Tsubaki, *ACS Catal.*, 2021, **11**, 11742-11753.
12.   S. Li, H. Guo, C. Luo, H. Zhang, L. Xiong, X. Chen and L. Ma, *Catal. Lett.*, 2013, **143**, 345-355.
13.   R. Yao, J. Wei, Q. Ge, J. Xu, Y. Han, Q. Ma, H. Xu and J. Sun, *Appl. Catal., B*, 2021, **298**, 120556.
14.   K. An, S. Zhang, J. Wang, Q. Liu, Z. Zhang and Y. Liu, *J. Energy Chem.*, 2021, **56**, 486-495.
15.   S. Liu, H. Zhou, Q. Song and Z. Ma, *J. Taiwan Inst. Chem. Eng.*, 2017, **76**, 18-26.
16.   S. Liu, H. Zhou, L. Zhang, Z. Ma and Y. Wang, *Chem. Eng. Technol.*, 2019, **42**, 962-970.